Springer

Journal of
Mechanical
Science and
Technology

Journal of Mechanical Science and Technology 23 (2009) 170~182

www.springerlink.com/content/1738-494x
DOI 10.1007/s12206-008-0717-x

Effect of partial rotor-to-stator rub on shaft vibration †

Mohamed. A. Abuzaid, Mohamed E. Eleshaky* and Mohamed G. Zedan

Department of Mechanical Engineering, College of Technological Studies
Public Authority for Applied Education & Training P.O. Box 42325, Shuwaikh, 70654, Kuwait

(Manuscript Received January 2, 2008; Revised June 30, 2008; Accepted July 19, 2008)

Abstract

The effect of partial rotor-to-stator rubbing is investigated both experimentally and analytically. It is found that due to rubbing the measured vibration signal is distorted showing a flattened portion in the waveform. Spectral analysis indicates that the synchronous component is generally attenuated as a result of rubbing-introduced-friction. It is also indicated that light rubbing induced vibrations are characterized by harmonics at frequencies equal to 1x rev., 2x rev., and 3x rev. Whereas, severe rubbing is identified experimentally by a spectrum containing subharmonics at 1/3 and 2/3 of the rotational frequency. Because of the stiffening effect of rubbing on the rotor, the resonance frequency increases. In general, the analytical results show good agreement with experimental data.

Keywords: Rub; Partial Rubbing; Rotor; Rotordynamics; Vibrations

1. Introduction

Rubs are typically introduced by contact between rotating and stationary elements of a machine. Preserving ample clearances prevents rubbing from becoming a serious problem. However, very often a shaft is bent or lateral vibrations of a rotor become excessive. This results in a reduction of clearances and, as a consequence, rubbing takes place. Two extreme cases of rotor rubs may usually take place. The first case is the full annular rub which occurs when the rotor maintains contact with a stator (e.g., a seal) during a complete revolution. The second case is the partial rub which takes place when the contact occurs during a portion of the period of precession. Another type of rub which deserves mentioning is the so-called dry-whip or dry-friction backward whirl where the rotor rolls around inside the stator clearance like a planetary gear with an enormously high frequency. This latter case may occur, for example, when inducer vanes of open impellers radially strike the stationary shroud providing that the rotor flexibility allows this type of orbiting.

Generally, full rub is preceded by a partial rub. With partial rub onset, the rub point begins to act as a new dry non-lubricated bearing supporting the rotor. This new bearing introduces new physical phenomena as it modifies the dynamic characteristics of the system. These modifications are briefly in the form of an increase in the average spring constant of the rotor as well as an evolution of friction forces as a result of the relative motion between the stator and the rubbing rotor.

Vibrations generated by the running mechanism are very complex and may lead to total destruction of the machine in just few rotations. The rub-related vibrations in turbo-machinery have been documented in several publications [1-8]. As observed from the literature, a partial rotor/stator rub often causes a steady subharmonic at a frequency equal to half of the rotational speed. Bently [1], who examined the sub-synchronous frequency resulting from rotor rub, indi-

† This paper was recommended for publication in revised form by Associate Editor Eung-Soo Shin

* Corresponding author. Tel.: +965 9 954 5962, Fax: +965 2 532 0460
E-mail address: esheky@aim.com

cated that half rotational speed motion is a general consequence of a rotor running at a speed equal to twice its natural frequency. He interpreted this experimental finding in terms of analytical results using linear parametric excitation phenomena modeled by the Mathieu equation [2]. Later, Childs [3, 4] explained the 1/2 speed frequency response results obtained by Bently's [1] rub condition using a linear analysis based on the Jeffcott model. The study was concerned with whirling motion which occurred in rotors subjected to a rub caused by radial stiffness variation. His linear parametric analysis showed that, during rubbing condition, Coulomb damping significantly widens the potential range of unstable speed.

Other investigators studied the non-synchronous clearance effects. Ehrich and O'Connor [5] employed nonlinear simulations to explain the 1/2 frequency field data. Ehrich [6] employed nonlinear analysis and simulations to explain the sum and difference frequency phenomena, reported by his experimental investigations. Both rotor units examined by Ehrich were supported by roller bearings.

In an attempt to describe the physical phenomenon related to rotor rub, Musznska [7] presented experimentally complex orbit patterns for a heavy rub condition. She also analyzed theoretically the light rub. The rotor response presented in her study showed that steady state subharmonic vibrations in the order of 1/2, 1/3, and 1/4 of the rotational frequency may exist as a result of rotor transient free lateral vibrations. For the case of light rubbing, Beatty [8] provided a reliable detection method based on the relative harmonic frequency strength.

Choi and Noah [9] investigated the rub problem as a piecewise linear vibration problem and proposed an algorithm to calculate the steady state solution using the fast Fourier transform (FFT) technique. They showed that subharmonics and super-harmonics could be found due to rubbing. Crandall and lingener [10] showed experimentally the reverse whirling of a flexible rotor and introduced a theory to explain backward rolling and backward slipping in case of rubbing. Choi [11] demonstrated a rubbing phenomenon which has different forms with the increase and decrease of the operating speed and explained the onset of backward precession. Choi [12] also studied experimentally the partial rotor-rub against a stationary element. He showed several partial rubbing phenomena of super-harmonics and sub-harmonics. Choi also calculated the orbit patterns of the forward and backward whirling.

The objective of the present study is to carry out experimental and analytical investigations in order to gain some insight into the diagnostics of rotor-stator rub conditions. A setup was built to carry out experiments on a rotor bearing system. The experimental observations are used to propose a mathematical model for rub identification. The analysis provides a few modifications to the mathematical models presented by Childs [3, 4] and Musznska [7] for the same problem. Modifications of rotor stiffness caused by contact with the rotor housing are introduced in terms of a nonlinear function added to the equation of motion. Similarly, the frictional force developed as a result of the relative motion between rubbing elements is expressed in a nonlinear form. Unlike Beatty's model [8], which assumed a rigid casing, the housing in the present analysis is treated as a flexible member.

2. Experimental work

2.1 Experimental apparatus

Shown in Fig. 1(a) is a schematic of the test rig used in the present study. The rig consists of a heavy rotor mounted centrally on a steel shaft having a Young's modulus of 200 GN/m^2. The rotor has a diameter of 70 mm, while the shaft has a uniform diameter of 18 mm. Two antifriction ball bearings are used to support the shaft. The span between the bearings is adjusted to 540 mm. The rotor assembly is driven by a D.C. motor capable of running the system up to 6000 rpm. The shaft is connected to the motor through a steel spring which acts as a flexible coupling. Four rubber mounts are used to isolate the vibration generated by the system from being transmitted to the foundation. To carry out rub experiments, a brass cantilever angle is bolted to the rotor casing. By controlling the clearance between the cantilever and the rotor, different conditions of rubbing are created.

An electrodynamic velocity pickup has been used to measure the vibration of the stationary component. The absolute displacement is calculated by the time integration of the sensed absolute velocity of the pickup. Shaft vibration measurements relative to the base are collected with a non-contact eddy current proximity probe. Time domain signals are displayed on a two channel oscilloscope. The outer circumference of the rotor is divided into 36 equal divisions so that the angular location of the unbalance present in the rotor is determined. The quartz controlled fre-

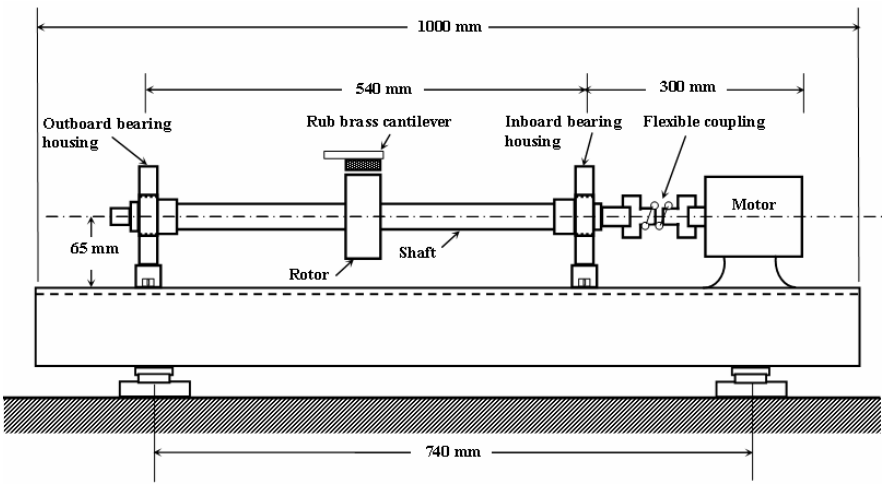

(a)

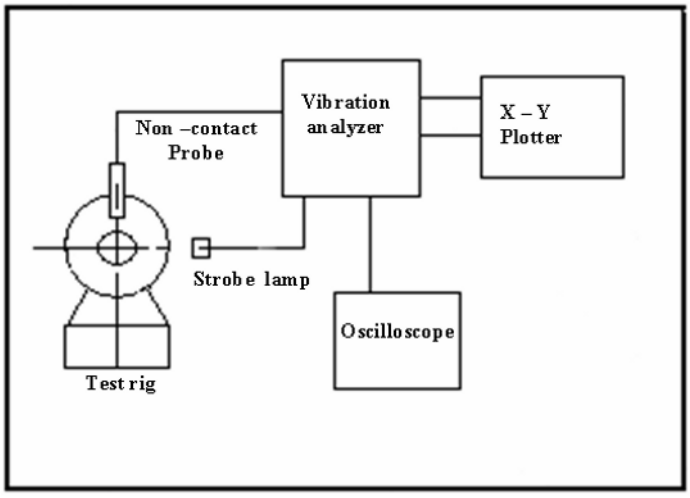

(b)

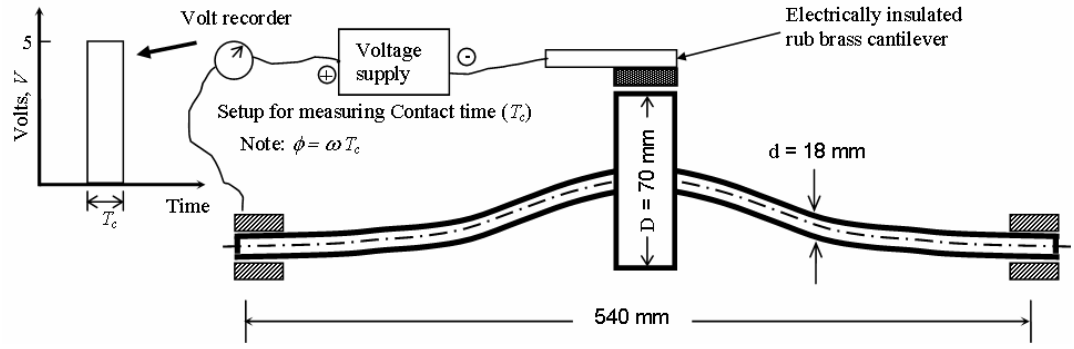

(c)

Fig. 1. (a) Schematic of the test rig, (b) Block diagram of the test rig, and (c) Measurment principle of rubbing contact angle.

quency generator and the high intensity strobe lamp on the vibration analyzer make it possible to measure the unbalance angular location and the shaft rotational speed as well. A block diagram of the experiment setup is shown in Fig. 1(b).

In the analysis of rub-related phenomena, the rubbing contact angle (ϕ) plays an important role. This angle is related to the contact time (T_C) through the relation, $\phi = \omega T_C$. In order to experimentally obtain the rubbing contact angle, a time contact sensor was built. Its measurement principle can be easily understood from Fig. 1(c). An electrically insulated brass cantilever and rotor are supplied with a constant voltage. During contact with the brass cantilever the voltage changes as indicated in the figure and the rubbing contact angle can be easily computed.

The rotor system modal parameters (mass, damping, stiffness) are identified by using a synchronous perturbation technique, Musznska [13], in which a controlled unbalance (m) is added to the rotor at a known location (r) and the resulting synchronous response (A) is measured. The observed modal mass and modal stiffness are identified from the natural frequency $\left(\omega_n = \sqrt{K_o / M}\right)$ and the direct synchronous dynamic stiffness $\{K_o - M\omega^2 = [mr\,\omega^2\cos(\delta - \alpha)]/A\}$. Whereas, the modal damping coefficient is identified from the quadrature synchronous dynamic stiffness $\{C\omega = [mr\,\omega^2 \sin(\delta - \alpha)]/A\}$. The rotor system modal parameters obtained in the present study are shown in Table 1.

2.2 Experimental results

To investigate the rubbing induced forces and their effect on rotor vibrations, two sets of experiments were run. In the first set, no rubbing condition takes place and the rotor dynamic characteristics are determined from the vibration measurements. In the second set of experiments, the brass angle is put in place and measurements are taken for the rub condition. In the following sections both cases are described and discussed.

Table 1. Modal parameters of the rotor system.

Mass, M (kg)	1.68
Stiffness, K (N/m)	314,159
Damping Coefficient, C (N/(m/s))	87
Eccentricity, r_e (μm)	6.23

2.2.1 No rubbing condition

A non-contact probe is located vertically 3 mm away from the mid-span rotor. The probe is attached to the base of the rig where the bearing blocks and the driving motor are directly mounted. Vibration measurements of the shaft in terms of peak to peak (P-P) displacement are obtained at different speeds. Results from the baseline are presented in Fig. 2 and Fig. 3. Fig. 2(a) shows the probe output at speed 2800 rpm. Frequency analysis for this time base signal is shown in Fig. 2(b).

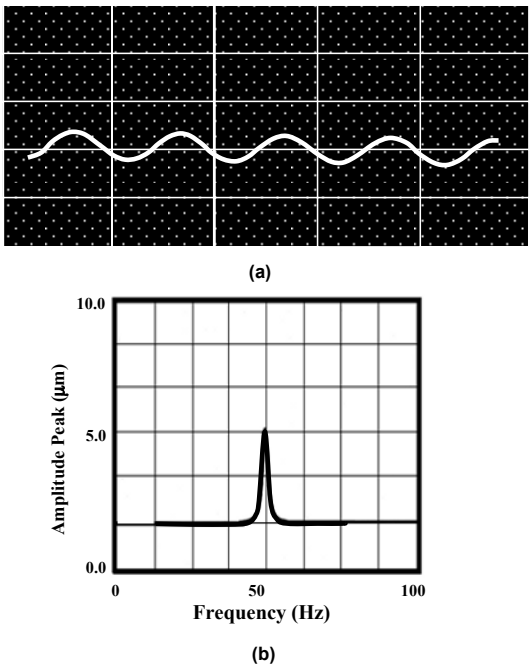

Fig. 2. (a) Shaft unbalance waveform – vertical response and (b) Response in frequency domain (Speed =2800 rpm).

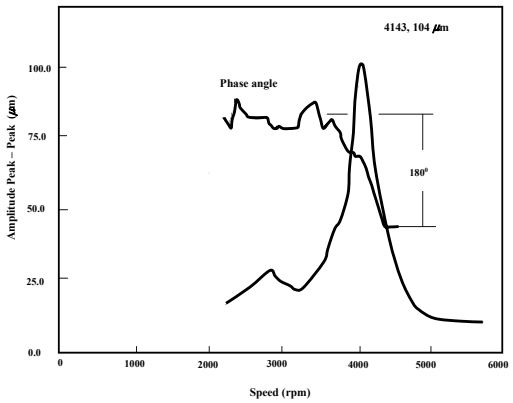

Fig. 3. Rotor vibration response (No Rubbing).

Fig. 3 presents the synchronous vertical response of the rotor as a function of speed. The variation of phase angle with speed is also plotted on the same figure. The critical speed of the shaft is found to be 4143 rpm as shown in the figure where a large peak amplitude, associated with a phase shift of 90° is observed. As can be seen from the figure, once the critical speed passes, the amplitude of vibration decreases and an 180° phase shift is detected. The experimental data described above indicates that the unbalance present in the system is the source of the above vibrations. This is verified by the sinusoidal shape of the recorded time base signals as well as the synchronous response shown by the spectral analyses of these signals.

2.2.2 Operation with rubbing onset

For rub experiments, the clearance between the brass cantilever and the rotor is adjusted to set different conditions of rubbing. The oscilloscope picture shown in Fig. 4(a) was taken while rubbing was applied to the system. The shaft rotational speed was set at 2400 rpm. As can be seen, a waveform characterized by a flattened shape is detected. The spectral analysis of this signal (Fig. 4(b)) shows an increase in the magnitude of frequency components. Fig. 5(a) is another oscilloscopic picture of rotor vibration taken at a relatively higher speed, 3900 rpm. The resulting motion is steady and periodic. The spectral analysis shown in Fig. 5(b) indicates a reduction in the magnitude of the second harmonic and the disappearance of higher frequency components. This can be explained by the fact that the length of the contact arc (= rubbing contact angle x Rotor radius) increases as the rotor speed increases. This is associated with a decrease in average angular variation of rotor radial stiffness due to the contact with the stator. Should the rubbing angle ultimately approach 360°, the average rotor stiffness variation is brought to zero.

Fig. 6(a) and Fig. 6(b) are the waveform and the frequency spectrum registered at a rotational speed of 4400 rpm. It should be noted that the Real Time Data Analyzer used for the present frequency spectrum analyses has three bandwidth settings: 45 cpm, 150 cpm, and 450 cpm. The bandwidth was initially set to 150 cpm. At this setting, a great deal of high frequency vibration activity is noticed. In order to record the details of these vibrations, the bandwidth setting was changed to 45 cpm. As seen in Fig. 6(b), the resulting spectrum contains sub-synchronous vibration

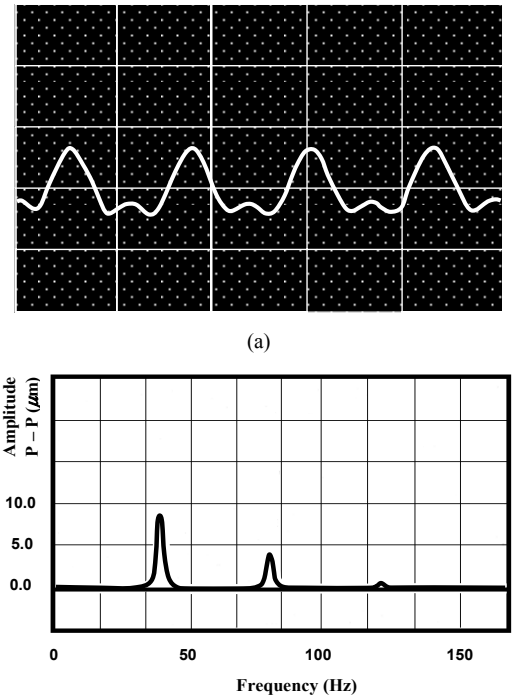

(a)

(b)

Fig. 4. Shaft under rubbing condition at 2400 rpm (a) Shaft vibration waveform and (b) Spectral analysis.

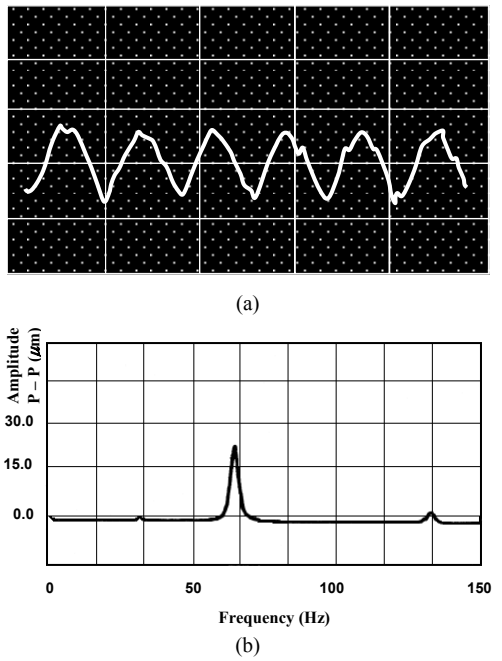

(a)

(b)

Fig. 5. Shaft under rubbing condition at 3900 rpm (a) Shaft vibration waveform and (b) Spectral analysis.

at 1/3 and 2/3 of the rotational frequency. Sub-synchronous vibration is also observed at a speed equal to 3900 rpm. In general, Figs. 5(b) and 6(b) indicate that, at high speeds, rubbing induced vibrations are not identified by a single frequency component but are rather distributed over relatively broad bands centralized by the synchronous frequency and its multiples. Two possible factors could lead to the appearance of vibration bands. The first is the friction forces which are, of course, a consequence of applied rubbing. These friction forces apply a frictional torque opposed to the rotor motion, resulting in a fluctuation of rotor speed. Therefore, the frequency spectrum would contain a vibration component corresponding to these modified precessional speeds. On the other hand, the transient vibration which follows the removal of the friction torque in the rub free zone could be another factor.

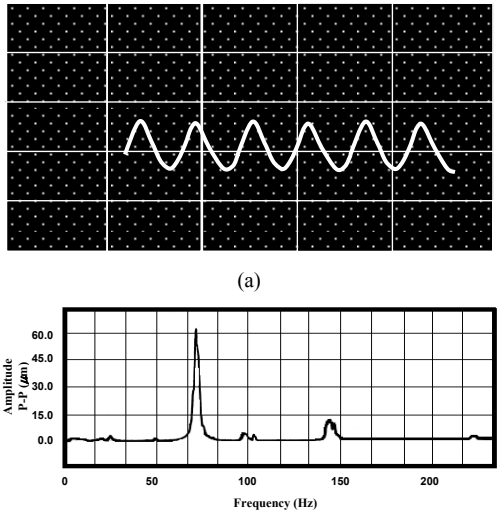

Fig. 6. Shaft under rubbing condition at 4400 rpm (a) Shaft vibration waveform and (b) Spectral analysis.

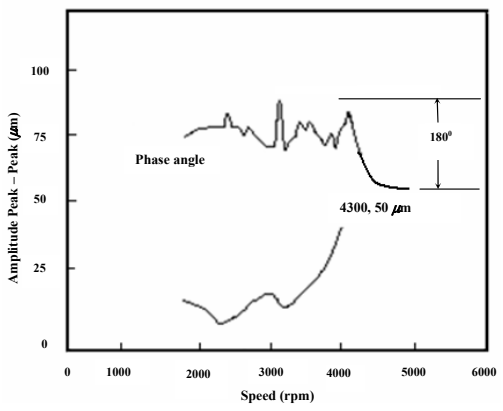

Fig. 7. Rotor vibration response under rubbing onset.

Synchronous response of the rotor measured as a function of speed is plotted in Fig. 7. The amplitude (peak-to-peak) is measured in μm and the phase angle refers to the vertical direction. During the experimental procedure, it is noticed that in the range from 4000 – 4200 rpm the rotor was running very rough, which made the vibration measurements difficult to collect as they were highly erratic. From the figure, it seems that rubbing has a big effect on the rotor response as the amplitude of vibration is largely attenuated in comparison to the case of no rub vibrations. It is also noticed that the critical speed of the rotor increases due to rubbing. The phase angle curve (Fig. 7) indicates that the critical speed is greater than 4400 rpm. Generally, the contact between the rotor and the stator increases the rotor dynamic stiffness. This increase in rotor stiffness increases the rotor critical speed.

3. Mathematical analysis

In order to gain more insight into the vibration that was producing rubbing mechanism and its effect on the response of rotating machinery, the above experimental investigation is complemented by an analytical study of the problem. In the analytical approach, a mathematical model is formulated and the resulting equations are solved for two cases: light rubbing and severe rubbing. The solution for the first case is determined by using a perturbation technique (multiple-scale method [2]), while a numerical solution is used for the second case.

3.1 Equation of Motion

Details of the rotor model used for the derivation of the equation of motion are depicted in Fig. 8. The model consists of a massless shaft having one rotor. Rubbing is applied to the rotor during a rubbing contact angle (ϕ). The onset of rubbing is denoted by an angle β, from the horizontal axis.

As a result of rubbing, the rotor is acted upon by two forces, F_r and F_t, as shown in Fig. 8. The transverse force F_r is due to the effect of the stiffness of the stator and can be expressed as:

$$F_r = -K_a(t)\, Z \tag{1}$$

where Z = x + *i* y, $i = \sqrt{-1}$, and $K_a(t)$ is the additional stiffness brought about due to rubbing. The rubbing between the rotor and the stator occurs only during a part, ϕ, of the complete revolution of the shaft. The additional stiffness is thus a discontinuous periodic phenomenon that can be represented by the periodic step function shown in Fig. 9. As mentioned in the presented experimental results, the increase in system stiffness due to rubbing is nonlinear. This has been verified by the distortion of the time domain signal and the appearance of super-harmonics and sub-harmonics as well. Therefore, it seems reasonable to assume the following shape function for the additional stiffness:

$$K_a(t) = K_s \left[a_o + \sum_{n=1}^{m} a_n \cos(n\omega t) \right] \tag{2}$$

where $a_o = \frac{\phi}{2\pi}$, $a_n = \frac{2}{n\pi}(-1)^n \sin\left(\frac{n\pi}{2}\right)$, ω is the exciting frequency (i.e., rotor speed) and K_s is the stator stiffness. The friction force, F_t induced by rubbing can be expressed as:

$$F_t = i\,\mu\, F_r \tag{3}$$

where μ is the coefficient of dry friction between the rubbing elements. The resultant force induced by rubbing is therefore given by:

$$F = F_r + F_t = F_r(1 + i\mu) \tag{4}$$

Using Eqs. (1) - (4), the equation of motion may be written in the following form:

$$M\ddot{Z} + C\dot{Z} + K_o Z + K_a(t)\,(1 + i\mu)\, Z = M r_e \omega^2 e^{iwt} \tag{5}$$

where *M, C, and* K_o are rotor mass, damping and stiffness coefficient, and r_e is the rotor eccentricity.

Substituting Eq. (2) into Eq. (5) and dividing by M gives:

$$\ddot{Z} + 2\varsigma\omega_n \dot{Z} + \omega_n^2 Z + \varepsilon\omega_n^2 \left[a_o + \sum_{n=1}^{m} a_n \cos(n\omega t) \right](1 + i\mu) Z = r_e \omega^2 e^{i\omega t} \tag{6}$$

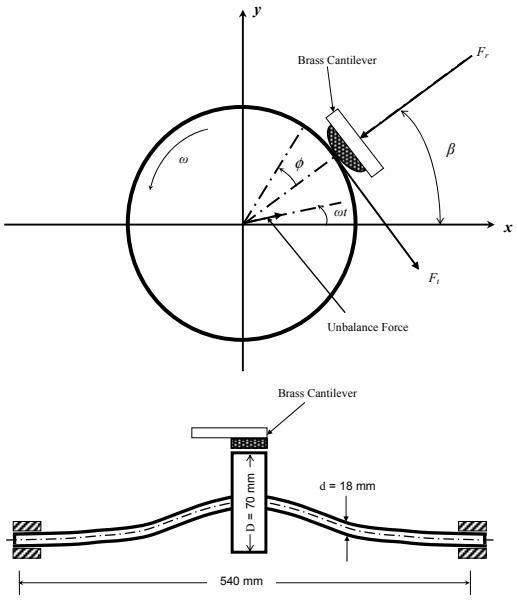

Fig. 8. Schematic of rotor modeling.

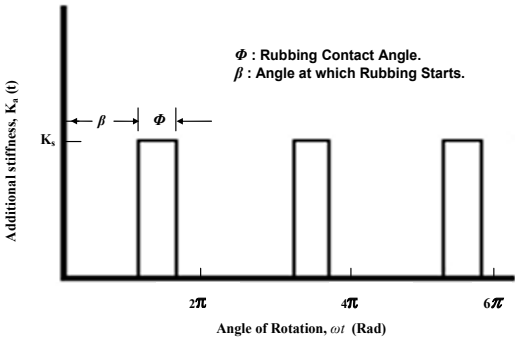

Fig. 9. Variation of Additional Rotor Stiffness with the Angle of Rotation.

where $\varepsilon = \frac{K_s}{K_o}$, $\omega_n^2 = \frac{K_o}{M}$ and $\varsigma = \frac{C}{2M\omega_n}$.

In the case of light rubbing, it is assumed that ε is small; thus the solution to Eq. (6) can be considered as a perturbation of the solution of the following simple equation:

$$\ddot{Z} + 2\varsigma\omega_n \dot{Z} + \omega_n^2 Z = r_e \omega^2 e^{(i\omega t)} \tag{7}$$

The solution to Eq. (7) is obtained by using a perturbation technique usually referred to as the method of multiple scales. In this method, the rotor response is expressed by the following asymptotic expression:

$$Z = Z_o + \varepsilon Z_1 + \varepsilon^2 Z_2 \tag{8}$$

and introducing new independent variables:

$$T_n = \varepsilon^n t \quad \text{for} \quad n = 0, 1, 2, \ldots\ldots\ldots$$

It follows that the derivatives w.r.t. t become expansions in terms of the partial derivatives w.r.t. T_n according to:

$$\frac{d}{dt} = D_o + \varepsilon D_1 + \ldots\ldots\ldots \tag{9}$$

Substituting (8) and (9) into (6), one gets after some manipulations:

For order ε^0

$$D_0^2 Z_0 + 2\varsigma\omega_n D_0 Z_0 + \omega_n^2 Z_0 = r_e \omega^2 e^{(i\omega t)} \tag{10}$$

For order ε^1

$$D_0^2 Z_1 + 2 D_0 D_1 Z_0 + 2\varsigma\omega_n (D_0 Z_1 + D_1 Z_0) + \omega_n^2 Z_1 = \omega_n^2 \left[\mathrm{a_o} + \sum_{n=1}^{m} a_n \cos(n\omega t) \right] (1 + i\mu) Z_0 \tag{11}$$

Eqs. (10) and (11) can be directly solved to yield

$$Z_0 = \frac{r_e \omega^2}{(\omega_n^2 - \omega^2) + 2i\varsigma\omega_n \omega} e^{(i\omega t)} \tag{12}$$

and

$$Z_1 = a_o C_1 e^{(iwt)} + \sum_{n=1}^{N} \left[A_n e^{i(n+1)wt} + B_n e^{-i(n-1)wt} \right] \tag{13}$$

where

$$A_n = \frac{a_n}{2^{n-1}} C_1 \left(1 + n(i)^{1-n} C_2\right)$$

$$B_n = \frac{a_n}{2^{n-1}} C_1 \left(1 - n(i)^{1-n} C_2\right)$$

$$C_1 = \frac{-r_e \omega_n^2 \omega^2 (1 + \mathrm{i}\mu)}{\left[\left(\omega_n^2 - \omega^2\right) + 2i\varsigma\omega_n\omega\right]^2}$$

$$C_2 = \frac{-2\varsigma\omega_n\omega}{\left[\left(\omega_n^2 - \omega^2\right) - 2i\varsigma\omega_n\omega\right]}$$

3.2 Analytical results

3.2.1 Light rubbing condition

The present predicted results for no- and light-rubbing conditions are shown in Fig. 10 and Fig. 11. System parameters used under these conditions are shown in these figures and in Table 1. Fig. 10(a) illustrates for rotor speed of 2800 rpm, the unbalance response of the rotor in case of no rub condition. As shown from the predicted results, a pure sinusoidal time wave is obtained. This result is quite close to the experimental observations obtained at the same speed (Fig. 2(a)) in terms of the vibration amplitude.

The vibration signal of the shaft exposed to light rubbing at speed 2400 rpm ($\omega/\omega_n = 0.58$) is illustrated in Fig. 10(b). Effect of rubbing is shown by a discrepancy of the lower part of the signal. This discrepancy is similar to the one seen in the experimentally obtained waveform presented in Fig. 4(a). This result gives an indication of the effect of the partial rubbing when applied to the shaft. It should be noted here that the brass cantilever clearance was adjusted in all experiments in such a way that keeps the rubbing contact angle fixed at 45°. Fig. 10(c) shows the predicted results for rotor speed of 3900 rpm. A flatness of wave at the peak and a discrepancy at the valley are clearly shown in these figures and are due to an increase in the effective rotor dynamic stiffness as a result of the increased rotor speed. It is believed that this discrepancy is also due to sub- and super-harmonics shown experimentally in Fig. 5. The result for high speed of 4400 rpm is presented in Fig. 10(d). The effect of rubbing on the waveform is less significant and the waveform is not sinusoidal as expected. The discontinuity shown is a result of rub onset, which is comparable with the experimental waveform shown in Fig. 6(a).

A parametric study for the system parameters ε, ω/ω_n, and ϕ is shown in Fig. 11. Fig. 11(a) illustrates the effect of additional stiffness ratio (ε) on the rubbing vibration. The vibration signal is seen to deviate from the no rub condition. As ε increases, the distortion of the waveform increases, which indicates the presence of higher harmonics in the vibration signal. Fig. 11(b) shows the effect of shaft speed (ω/ω_n) on the rubbing induced vibration waveform. As can be seen, when the shaft is running away from critical speed, the vibration waveform is not greatly affected by rubbing. However, when the shaft speed

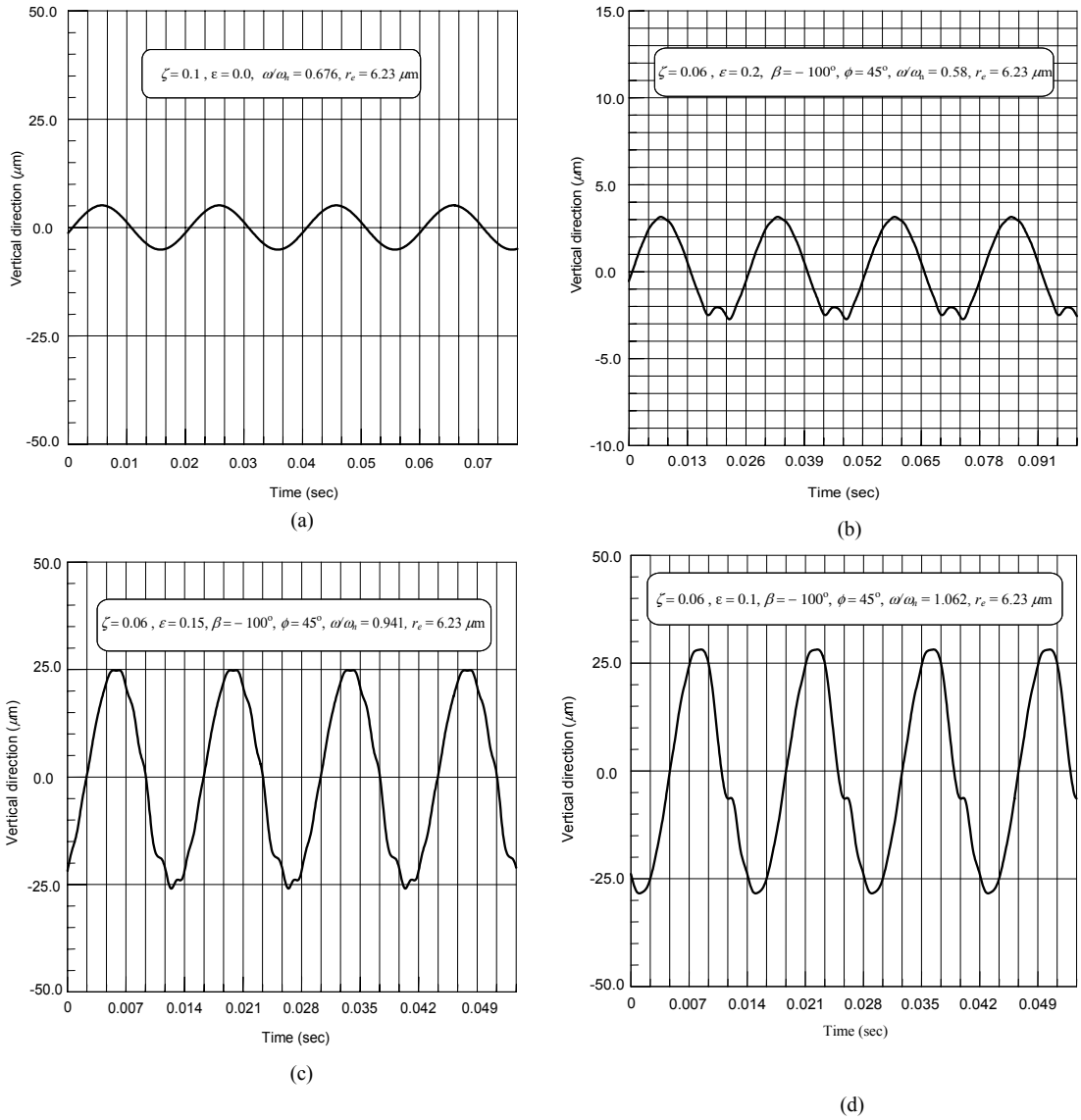

Fig. 10. (a) Predicted shaft vibration response for no rub condition; predicted shaft vibration response for light rub condition at different speeds (b) 2400 rpm, (c) 3900 rpm, and (d) 4400 rpm.

is close to its critical speed ($\omega/\omega_n \approx 0.943$), the vibration amplitude is increased and the waveform is obviously distorted as a result of the light rub onset. Fig. 11(c) shows the shaft vibration waveform for rubbing contact angles (ϕ) of 10^o, 45^o, and 90^o. The vibration waveform is obviously distorted during the contact arc. However, away from the contact arc, very little distortion is observed, giving an indication that light rubbing is a localized phenomenon.

3.2.2 Heavy rubbing condition

In the following section, the dynamics of rotating machines when subjected to severe rubbing are studied. Under this condition, the nonlinear rubbing forces have a dominant effect on system synchronous vibration normally generated by an unbalanced force. Therefore, the solution of the equation of motion (6) cannot be assumed to be a perturbation about system synchronous response as in the case of light rubbing

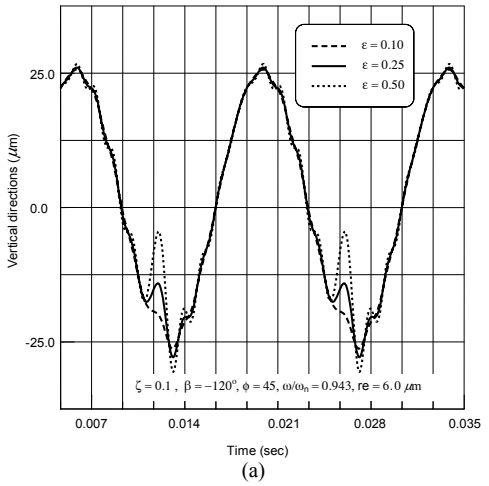

(a)

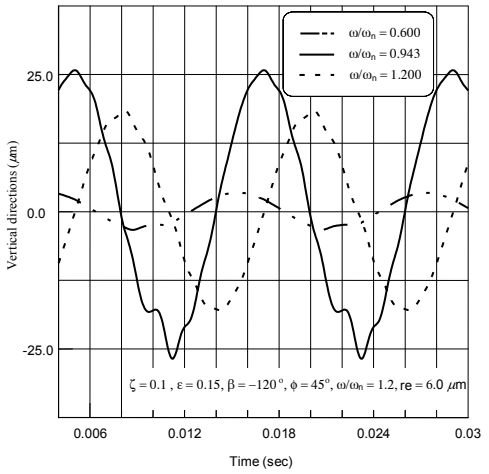

(b)

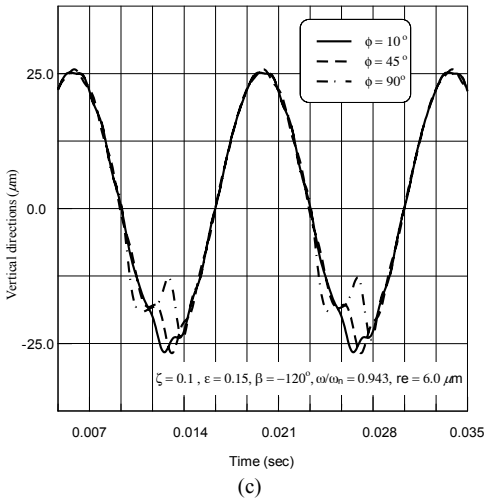

(c)

Fig. 11. Rubbing induced vibration waveform at different parameters: (a) ε , (b) ω/ω_n , and (c) ϕ .

previously analyzed. Analytical solution of this problem using the perturbation method definitely yields erroneous results. Hence, the rotor response in this case is obtained by using a numerical technique. The Runge-Kutta method with Gill's modification [14] is used to integrate the differential equation of motion (6) w.r.t. time. The utilized Gill's modification is intended to adjust the size of the final value of the response with a minimum time for a given accuracy. The time of integration is determined by obtaining a steady state solution if it exists.

It is obvious that many system parameters, such as stiffness ratio, damping coefficient, rubbing contact angle and contact angular location may affect the rotor response. However, the present study is concerned only with the effect of the rubbing arc (rubbing contact angle) on rotor response. Therefore, rotor response vibration as a function of time is calculated at a rotor speed equal to 390 rad/s for different values of the rubbing contact angle. Size of integration step is selected as 0.00075 second, and the maximum allowed error in rotor response is 0.5% of the shaft

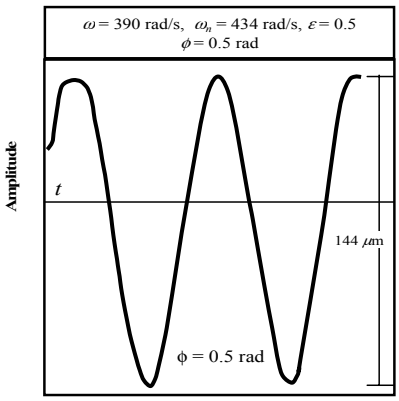

(a)

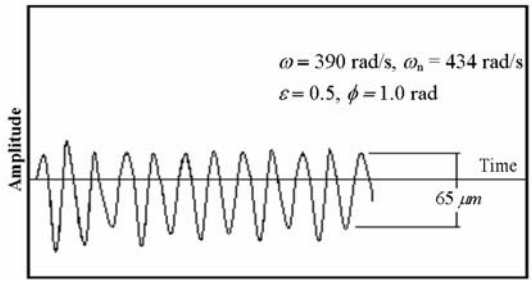

(b)

Fig. 12. Predicted vibration time signal (a) ϕ = 0.5 rad and (b) ϕ = 1.0 rad.

eccentricity (e). With the exception of the rubbing contact angle, the other parameters describing the system dynamic characteristics, such as, critical speed, stiffness ratio, damping coefficient and obstacle location remain unchanged. The effect of rubbing on system dynamics response is discussed by using time domain analysis as follows. Figs. 12(a) and 12(b) show the predicted rotor response versus time for two different rubbing contact angles 0.5 and 1.0 radians, respectively. These figures describe the rubbing progress from initial stage to the eventual rotor instability as the rubbing arc increases. It is clearly seen that the waveform is largely affected by contact arc length. The figures show times trace having a flattened portion. This flattened portion indicates the presence of rubbing forces in the system as shown previously in the experimental analysis.

Based on the predicted response, it is noticed that the rubbing duration has an effect on the peak to peak amplitudes. Friction force due to rubbing introduces to the system a Coulomb type of damping which helps attenuate the vibration amplitude of the rotor. Figs.12(a) and 12(b) indicate that vibration amplitude dropped from 144 to 65 μm as the rubbing contact angle is increased from 0.5 to 1.0 radian. It should be noticed that, for no rub condition (ϕ=0), the amplitude of vibration calculated at the same speed is 213 μm.

Shaft orbits are obtained for the above two rubbing contact angles by using the numerically calculated response in both horizontal and vertical orbits (Figs.13(a) and 13(b)). The figures indicate that orbits are significantly distorted by introducing rubbing into the system. The banana-shaped orbit obtained for a rubbing contact angle of 0.5 radian is gradually modified to a semi elliptic shape when the rubbing contact angle increases to one radian.

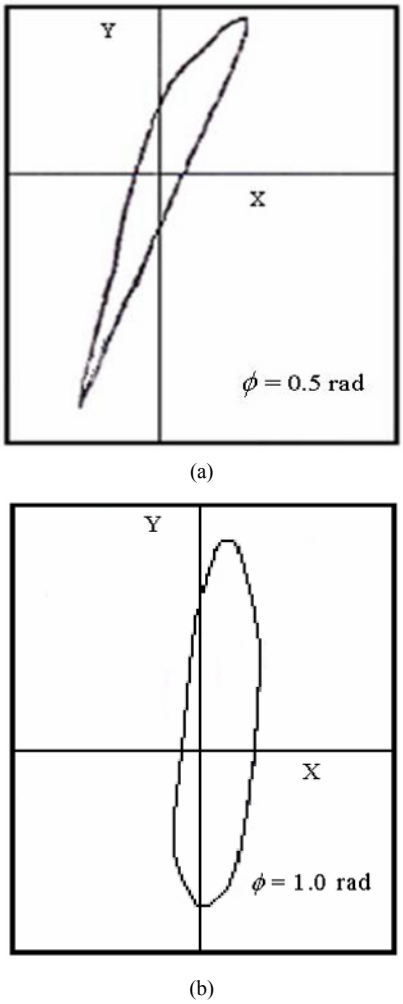

Fig. 13. Orbit plot (a) ϕ = 0.5 rad and (b) ϕ = 1.0 rad.

4. Conclusions

From the experimental and analytical results, the following conclusions are drawn:

(a) The numerically predicted waveform shows a considerable resemblance to the experimentally obtained rotor rubbing response. This resemblance is demonstrated in the flattened portion of the time domain response. This is considered a significant characteristic that identifies rubs experienced by rotating machines.

(b) Shaft precessing orbits are largely distorted due to rubbing. In addition, the phase angles of synchronous amplitudes are greatly modified. Hence both orbits and phase angles are major parameters to diagnose rubbing rotors.

(c) Friction forces associated with rubbing introduce dry damping effect into the system, which leads to the attenuation of synchronous vibration amplitudes.

(d) Spectral analysis has shown that rubbing onset may best be examined by observing super-harmonics and sub-harmonics as well. Synchronous component proved to be misleading in this aspect.

(e) Rubbing contact angle is a very important parameter to analyze if it is required to investi-

gate rotor instability. In the present analysis, a rubbing contact angle of 90^o is found to be a separation point between non-destructive and destructive rubbing. This angle is expected to vary as system dynamic characteristics vary. Further work is required to provide data about the relation between rubbing contact angle and other system parameters such as stator stiffness, rotor speed, etc.

References

[1] D. E. Bently, Forced Subrotative Speed Dynamic Action of Rotating Machinery, *ASME Publication 74-Pet-16, Petroleum Mechanical Engineering Conference,* Dallas, TX, (1974).

[2] A. H. Nayfeh, *Nonlinear Oscillation,* Wiley-Interscience Publication (1979).

[3] D. W. Childs, Rub-Induced Parametric Excitation in Rotors, *The University of Louisville, Kentucky, Report* (1980).

[4] D. W. Childs, Fractional-Frequency Rotor Motion Due to Nonsymmetric Clearance Effects, *ASME Publications 81-GT-145, International Gas Turbine Conference and Products Show,* Huston, Texas, March (1981).

[5] F. F. Ehrich and J. J. O'Connor, Stator Whirl with Rotors in Bearing Clearance, *ASME WA/MD-8,* Paper 66 (1966).

[6] F. F. Ehrich, The Dynamic Stability of Rotor-Stator Radial Rubs in Rotating Machinery, *Paper ASME,* 56 (6) (1969).

[7] A. Muzynska, Partial Lateral Rotor to Stator Rubs, in proceeding Vibration in Rotating Machinery, *IMechE C281/84, Institution of Mechanical Engineers,* (September) (1984) 327-335.

[8] R. F. Beatty, Differentiating Rotor Response due to Radial Rubbing, *Journal of Vibration Acoustics, Stress and Reliability in Design,* 107 (April) (1985) 151-160.

[9] Y-S. Choi, and S. T. Noah, Nonlinear Steady-State Response of a Rotor-Support System, *Journal of Vibration, Acoustics, Stress and Reliability in Design,* 109 (4) (1987) 225-261.

[10] S. H. Crandall and A. Lingener, Experimental investigation of Reverse whirl of a flexible Rotor, *Third International Conference on Rotor Dynamics, Lyon,* France, (1990) 13-18.

[11] Y-S. Choi, Dynamics of Rotor Rub in Annular Clearance with Experimental evaluation, *KSME Journal,* 8 (4) (1994) 404-413.

[12] Y-S. Choi, Experimental Investigation Of Partial-Rotor Rub against a Non-Rotating Part, *Seventh International Conference on Vibrations in Rotating machinery,* University of Nottingham, UK, IMechE C576/033/2000, (September) (2000) 281-290.

[13] A. Muzynska, Vibrational Diagnostics of Rotating Machinery Malfunctions, *International Journal of Rotating Machinery*, 1 (3-4) (1995) 237-266.

[14] C. F. Gerald, *Applied Numerical Analysis,* Addison-Wesley Publication Company, New York, USA, (1970).

Mohamed A. Abuzaid received his B.S. degree in Mechanical Engineering from Cairo University, Cairo, Egypt, in 1970. He then went on to receive his M. Eng. degree from Carleton University, Ottawa, Canada in 1979, and his Ph.D. degree from Cairo University, Egypt in 1987. Dr. Abuzaid is currently a lecturer at the Department of Mechanical Engineering Technology at the Public Authority for Applied Education & Training in Kuwait.. His research interests are in the area of dynamics of rotating machines.

Mohamed E. Eleshaky received his B.Sc. and M.Sc. degrees in Mechanical Engineering from Alexandria University, Alexandria, Egypt, in 1982 and 1987, respectively. He then went on to receive a Ph.D. degree from Old Dominion University, Virginia, U.S.A in 1992. Dr. Eleshaky is currently an Assistant Professor at the Department of Mechanical Engineering Technology at the Public Authority for Applied Education & Training in Kuwait. He is also on leave from the Mechanical Engineering Department, Faculty of Engineering, Alexandria University, Egypt. His research interests are in the areas of aerodynamic design optimization and sensitivity analysis, computational fluid dynamics, jet flows, tribology, and vibrations.

Mohamed G. Zedan is an assistant professor in the Mechanical Engineering Dept., College of Technological Studies, Kuwait. He was a Staff Engineer in the gas turbine engine department, Textron Lycoming, Stratford, CT, U.S.A. He was a Sr. Research Engineer in the gas turbine engine department, Allison Gas Turbine GMC, IN, U.S.A. He has a B.Sc. degree in Mechanical Engineering from Cairo University, Egypt. He has a M.Sc. and Ph.D degrees in Mechanical Engineering from University of Waterloo, Canada.